Simultaneous, single particle, magnetization and size measurements of micron sized, magnetic particles

Jie Xu[a], **Kalpesh Mahajan**, **Wei Xue**, **Jessica O. Winter**[a], **Maciej Zborowski**[b], and **Jeffrey J. Chalmers**[a]

[a]William G Lowrie Department of Chemical and Biomolecular Engineering, The Ohio State University, 140 W. 19th Avenue, Columbus, OH 43210

[b]Department of Biomedical Engineering, Cleveland Clinic, 9500 Euclid Avenue, Cleveland, OH 44195

Abstract

Single particle magnetization and size measurements of micron and nano sized, magnetic particles were made using a previously described device referred to as Cell Tracking Velocimetry, CTV. Three types of commercially available, and commonly used, magnetic particles were studied in this report. While the CTV instrument provides individual particles measurements, the average magnetization and size measurements were found to have reasonable agreements with reported values from instruments which measure bulk values. In addition, the CTV instrument, using electromagnets, can also determine magnetization curves, which also proved to have reasonable agreement with other published studies. Given that magnetic separation and analysis technology is dependent on the quality of the magnetic particles used, studies such as this one using CTV provide not only average data, but also provides information with respect to the distribution of the properties such as magnetization and size. For example, the spread of the data in magnetic and settling velocities were found to be predominately due to the size distribution of the analyzed particles.

Keywords

Magnetophoretic mobility; particle settling velocity; particle magnetic velocity; cell tracking velocimetry; magnetization

The continued maturation of magnetic separation and analysis technology requires, for some applications, higher system performance. Typical performance metrics include a very high purity and recovery of the targeted cells or a high level of removal of undesired cells while still recovering the majority of desired cells. For example, to conduct a mismatched, bone marrow transplant, it is generally accepted that a 4 to 5 $\log_{10}$ depletion of the undesirable T cells from the donor sample is needed; yet to be practical, at least a 80 to 90% recovery of the desirable hematopoietic stem cells is also needed [1]. A second example is the use of magnetic cell separation technology for positive selection, or negative depletion, to enrich

for circulating tumor cells [2, 3]. In addition to magnetic cell separation, the use of magnetic particles for both the separation and detection of molecules is also growing [4–6].

A number of factors are involved in the optimization of magnetic separation and analysis technology; however, a fundamental part is the magnetic particles used to impart significant, magnetic moments to the targeted cells. An exception with respect to the use of these magnetic particles are cells that are intrinsically magnetic such as deoxygenated red blood cells, magnetic bacteria, and magnetic spores [7–10]. Commercial, magnetic particles typically range in diameter from on the order of 100 nm to 5 to 6 microns and consist of small, ~10 to 50 nm iron oxide nanocrystals contained within an organic polymer, typically some type of carbohydrate. There does exist, however, some larger particles in which the carbohydrate is replaced with a plastic or silica [11]. It is also possible, but not common, to move and potentially separate, diamagnetic particles (including cells) in solutions that are magnetic [12]. Factors specific to the particles that can significantly affect magnetic cell separation include the homogeneity, or lack thereof, of both this magnetic moment and particle size. A third consideration with respect to the performance of magnetic cell separation systems is the potential of magnetic particles to non-specifically bind to, or be internalized by, non-targeted cells [13].

The actual volume percent of magnetically susceptible material (i.e. iron oxides) in typical magnetic particles is usually a small fraction of the total particle volume [12–14]. Whereas average values of magnetization and size can be determined with current commercial instrumentation (i.e. SQUID, vibrating magnetometer, coulter counters), we know of no instrument that can measure these values on a particle-by-particle basis. In this report, we demonstrate measurement of particle magnetization and size on single, micron-sized particles and present a proof of concept plot of on the order 35 nanometer magnetic quantum dots.

Theory

As presented theoretically and experimentally by Jin et al. [12], the magnetically induced velocity of diamagnetic, paramagnetic, and superparamagnetic magnetic particles or cells in a magnetic energy gradient, S_m, is given by:

$$u_{mag} = \frac{\left(\chi_{particle} - \chi_f\right) D_{part}^2}{18\eta} S_m. \tag{1}$$

The magnetic energy gradient, S_m (T-A/mm^2), can be represented by:

$$S_m = \frac{d}{dx}\left(\frac{(B(x))_0^2}{2\mu_0}\right) = \frac{1}{2\mu_0}\frac{d(B(x))_0^2}{dx} = \frac{1}{2}\mu_0\frac{d(H(x))^2}{dx} \tag{2}$$

where B is the magnetic field induction (T), H is the strength of the applied magnetic field (A/m), μ_0 is the magnetic permeability of a vacuum: $4\pi \times 10^{-7}$ T m A^{-1}, and $B_0 = \mu_0 H$ (S.I units used in this report).

Similarly, the settling velocity u_{setl} of a cell or particle is defined by:

$$u_{setl} = \frac{\left(\rho_{sphere} - \rho_f\right) D_{part}^2 g}{18\eta}. \tag{3}$$

Dividing Equation 1 by 3, one obtains:

$$\frac{u_{mag}}{u_{setl}} = \frac{\left(\chi_{particle} - \chi_f\right)}{\Delta\rho g} S_m.$$

(4)

Jin et al. [7, 12] experimentally demonstrated in an instrument referred to as cell tracking velocimetry, CTV, Equation 4 is valid for polystyrene microspheres, *Bacillus* spores containing Mn, and oxygenated and deoxygenated red blood cells, over magnetic fields up to 1.2 T. This CTV instrument is able to determine both the settling velocity and magnetically induced velocity in a region of interest, ROI, which has a nearly constant value of S_m.

However, an assumption used to derive Equation 1 is that the magnetization, M (A/m), of the cell or particle of interest is directly proportional to the applied field:

$$\chi = \frac{M}{H}.$$

(5)

Whereas Jin et al. [12] demonstrated that this linear relationship of magnetization holds for polystyrene and biomass containing manganese over a range of 0 to 1.2 T, as expected, the magnetization of Fe_xO_y materials saturate at magnetic fields significantly below 1.2 T. Given the power of modern, permanent magnets, it is relatively straightforward to create magnetic field inductions greater than 0.1 T.

With this departure from linear behavior, one must consider the experimentally determined relationship defining the magnetization of Fe_xO_y material. Fundamentally, the magnetization, $M(B_0)$ for any material, diamagnetic, paramagnetic, or ferromagnetic, in an imposed magnetic field, is given by:

$$M(B_0) = \chi(H)H = \frac{\chi(H)B_0}{\mu_0}$$

(6)

Figure 1 is a plot of normalized magnetization ($M(B_0)/\rho$), as a function of magnetic field induction for two commonly used, commercial magnetic particles: Dynabeads M280 and M-450 (from [15]). Using X-ray diffraction, SEM analysis, Mossbaur spectroscopy, and a vibrating sample magnetometer, VSM, (used to make Figure 1), the authors reported that these two types of particles are predominately maghemite (γ-Fe_2O_3).

Figure 1 further demonstrates an approximate linear relationship between −0.05 T to 0.05 T, and the emergence of non-linear behavior above or below these values of *B*. In addition to maghemite, iron oxides can appear in a number of different forms, which can have significantly different magnetic susceptibilities and final, saturated magnetizations. Table 1 lists a number of relevant compounds to this study, including several iron oxide forms and values of magnetization.

Given this potential for non-linear behavior, the value of χ_p for a Fe_xO_y containing material in Equation 4, can be replaced with Equation 6, to obtain:

$$\frac{u_{mag}}{u_{setl}} = \frac{\left(\frac{\mu_0 M_s}{B_0} - \chi_f\right)}{\Delta\rho g} S_m$$

(7)

Further, given that microparticles are typically made of a carbohydrate and Fe_xO_y, the magnetization and density of the particles can be expanded to:

$$M(B_0)_{part}=w \bullet M(B_0)_{FexOy}+z \bullet M(B_0)_{carbohydrate} \qquad (8)$$

$$\rho_{part}=w \bullet \rho_{FexOy}+z \bullet \rho_{carbohydrate} \qquad (9)$$

$$1=w+z \qquad (10)$$

where w and z are the volume fraction of Fe_xO_y and carbohydrate/polymer, in the particles, respectively. It should be noted that the magnetization of a material, typically in units of A/m, is generally reported as a volume property.

We have previously described, calibrated, and experimentally demonstrated that the CTV instrument can measure the magnetically-induced velocity and sedimentation velocity of micron-sized particles and cells [12, 16–18]. In addition to the ability to quantify the intrinsic magnetic susceptibility of cells and particles and the amount of magnetic labeling on magnetically-labeled cells, Chalmers et al. 2010 and Sun et al. 2011 [9, 13] were able to demonstrate that the CTV system is sufficiently sensitive to be able to detect on the order of 5×10^{-15} gr of iron, in the form of Fe_3O_4, per cell and 1.16×10^{-11} gr of Mn in a single *Bacillus* spore. In this report, we demonstrate the ability of the CTV system to determine simultaneous size and magnetization measurements on single, commercially-produced magnetic microparticles and magnetic quantum dots believed to be on the order of 35 nanometers.

EXPERIMENTAL SECTION

Instrumentation

Less than one ml of cell/particle suspension (~5×10^5/ml) is needed to create histograms of magnetically induced velocity and settling velocity of several thousand distinctly analyzed cells or particles in the CTV apparatus. The most recent modification has resulted in another version of the instrument with electromagnets replacing permanent magnets, yet maintaining the same magnetic pole and sample chamber geometries [12]. Figure 2 presents a schematic diagram of the electromagnets and channel within which the region of interest is contain. This version of the instrument allows samples to be introduced into the sample chamber, the settling velocity to be determined, the magnetic energy gradient to be energized, and the magnetically induced velocity to be determined. Summarizing, the cell/particle suspension is introduced into the "region of interest", the injection flow is stopped, the settling of the particles is recorded using the computer imaging hardware and software, the magnetic field energized, and the movement of the cells/particle as a result of the magnetic energy gradient. These images are subsequently processed by the CTV software, and the tracked particle velocity is determined. Nakamura et al. [17] discussed the algorithm used to determine particle velocity as well as limits and sensitivity of the approach.

Particle Diameter determination

An independent microscopic system, Nikon 80i microscope with the NIS Elements BR research software, were used to estimate the diameter of the particles used in this study. A threshold was set based on background noise, and single particles were determined using a circularity gating (1.00 is perfect circle) to eliminate particle aggregates. Several hundred to over 1000 events were processed per particle type.

High viscosity solution

Aqueous glycerin solution was prepared using 60% weight of glycerin (Fisher Scientific) in distilled water. The viscosity of 8.96×10^{-3} kg/m-s was determined by a Brookfield DV-II + Viscometer at 25.0 °C, and the density of the solution was measured to be 1130 kg/m³ at 25.0 °C.

Particle Descriptions

Three types of beads were analyzed by the CTV system in this study: Dynabeads M280 (Dynabeads Streptavidin Trial Kit, Invitrogen 658.01D), Dynabeads M450 (Dynabeads CD3, Invitrogen 111.51D), and EasySep D magnetic particle (Stem Cell Technologies Inc. 19250). The magnetic particle solutions were washed with PBS/high viscosity solution once, then suspended in PBS/high viscosity solution at a concentration of 0.5×10^6 particles/mL.

As a proof of concept that sub-micron sized magnetic particles can be tracked in the CTV system, magnetic, quantum dot nanocontainers, of a nominal diameter of 35 nanometers, was also tested. The synthesis and initial characteristics was described previously (19).

RESULTS

Settling velocity vs. magnetic velocity

Figures 3 – 5 show the results of experimental analysis of EasySep™ D, Dynal M280 and M450 particles evaluated with the electromagnetic, CTV system (0.2A; B = 0.103 T; $S_m = 8.4 \times 10^5$ TA/m²). Figures 3A, 4A and 5A are dot plots of settling versus magnetic velocity (mm/s), whereas 3B, 3C, 4B, 4C, and 5B, 5C are histograms of settling and magnetic velocities, respectively.

While, generally speaking, Gaussian like distributions are observed in the velocity histograms, the general trend of a significant rise in magnetic velocity with increasing settling velocities, Figures 3A and 4A, raises the question of potential non-homogeneity in the particles. Specifically, inspection of Equation 4 indicates that the quotient of the magnetic and settling velocity should be a constant (i.e. not a function of particle size) if the particles are homogeneous with respect to composition and the magnetic field gradient is constant in the region of interest, ROI. In previous publications we reported that over the entire region of the ROI of the CTV instrument, the magnetic field gradient only changes by approximately 2 percent, and particles are typically only tracked over a part of the total region, confirming the assumption that the magnetic gradient is, essentially, constant [18]. Table 3 presents the mean and coefficient of variation of settling and magnetic velocity, and the quotient of magnetic and settling velocity (Equation 4 or 7), for each of the three particles.

Further inspection of Figures 5A–5C (Dynal M450 particles) and the CV values, both of the individual velocities, and the ratio of the velocities, indicates that a significantly higher amount of spread, compared to Figures 3A and 4A, is observed in the measured magnetically induced velocity. Previous experience with the CTV instrument, and actual visual observations of these studies indicated that if the particle/cell velocity is too high, these particles will not be viewed in the 5 frames needed to obtain a data point; hence a bias against faster particles can occur. This was theoretically and experimentally discussed in Nakamura et al. [17]. Consequently, M450 particles were suspended in a 60 percent glycerin solution, which creates a solution with a viscosity of 8.96×10^{-3} kg/m-s. Figures 6A through 6C presents experiments conducted in this solution and the reported CVs in Table 3 are significantly smaller compared to data presented in Figure 5.

Particle diameters

To provide independent measurements of particle diameter (relative to the CTV system), a microscopic, digital imaging system (Nikon 80i microscope and the NIS Elements BR research software) was used. (It should be noted that a significant number of particles are tracked by the CTV system that are out of focus; hence, independent particle size measurements were conducted in the Nikon microscope which placed the particles on a slide in the same focal plane). Figure 7A is a histogram of the diameter, in microns, of the Stem Cell Technologies EasySep™ magnetic particles (sample taken from same vial as used to make Figure 3). A total of 1,234 particles were analyzed automatically with the NIS software. To create this histogram, and to confirm only single particles, not clumps were counted, the "circularity" setting in the software was set for 0.95 (1.0 would be perfectly circular). The mean diameter was calculated to be 1.38 micron with a standard deviation of 0.674 micron. The sharp drop in particles of a diameter less than 0.517 micron suggest the particles were purified/collected with a filter of about 0.5 micron pour size during the manufacturing process. Figures 7B and 7C are similar histograms of the M280 and M450 Dynal particles, in which several hundred events were captured with a circularity setting greater than 0.30. With smaller CVs, these two types of Dynabeads appear to be more uniform in size. With these independently measured values of diameter, a mean density can be obtained by rearrange Equations 3:

$$\Delta\rho_{ave} = \frac{18\eta u_{setl,ave}}{gD^2_{part,ave}}$$

(11)

The visually measured diameter, and calculated density using Equation 11 is presented in Table 4.

Given the relatively large number of events that were recorded and analyzed in this study, one could use similar statistical methods as described previously [13] to fit the experimental data of the particle diameters to several distribution models. A normal (Gaussian) distribution model was used for Dynal M280 and M450, based on the visual observations of a Gaussian like distribution:

$$f(x,\mu,\sigma) = Ae^{\frac{-(x-\mu)^2}{2\sigma^2}}$$

(12)

where f is the probability density function, μ is the mean, σ is the standard deviation, and A is reciprocal of the interval used to create the given histogram.

With respect to the EasySep™ particles, a clear cut-off around 0.5 micron exists; consequently, a truncated normal distribution model was used which assumes that a pseudo-normal distribution lies within the interval $x \in (a, b)$, $-\infty$ $a < b$ ∞. The solid lines in Figure 7 superimposed on the interval plots are the predicted populations using the models described above. The numerical parameters presented in the figures represent the constants used in the models.

Particle Magnetizations

Given that the experimental output of the CTV instrument is the magnetically induced and settling velocity, u_{mag} and u_{setl}, Equation 7 can be rewritten to provide a particle by particle magnetization, or if average values of u_{mag} and u_{set} are used, an average magnetization of the population as a function of the quotient of these two experimentally determined velocities and values of the constants, S_m, B_o, g and μ_0:

$$M_s = \frac{B_0}{\mu_0}\left[\left(\frac{g\Delta\rho}{S_m}\right)\left(\frac{u_{mag}}{u_{setl}}\right)+\chi_f\right]. \tag{13}$$

Table 4 presents the average of the calculated magnetization for each of the particles tracked.

Knowing the magnetization of each particle, Equation 8 suggests that the actual amount of magnetic material within each particle can be estimated. As reported above, Fonnum et al. [15] experimentally demonstrated through X-ray analysis that the primary form of the iron in Dynal particles is maghemite (γ-Fe$_2$O$_3$). Independently, Woo et al. [20], and others, have reported that the bulk, saturated magnetization of maghemite is estimated to be 385 kA/m. In this current study, our magnetic field was 0.1 T which, according to Figure 1, corresponds to approximately 83% of the saturated magnetization. Given that the magnetic susceptibility of the carbon based polymer is nearly the same as the buffer, one can assume that the experimentally measured magnetization of the particle is solely due to maghemite. Table 4 lists the corresponding volume estimations of the particle that is maghemite, and using a density of 4.6×10^6 g/m^3, the number of grams of maghemite per particle. (Note, it is assumed that the EasySep D particles use maghemite). A similar calculation could be made based on the settling velocity; however the exact density of the polymer material in each particle is not accurately known.

Since an electromagnet is used in this study, and we have previously reported on the experimentally measured value of B and S_m within the ROI as a function of current [12], we attempted to determine the functional dependence of individual particle magnetization with applied field using varying current in the CTV apparatus. Assuming that the density of the M280 particles are constant, Equation 13 can be solved using the velocity data obtained for each particle. Equation 13 can be further reduced by the replacing of $\Delta\rho$ with Equation 11 to obtain the magnetization as only a function of the magnetically induced velocity:

$$M_s = \frac{B_0}{\mu_0}\left[\left(\frac{18\eta}{D^2 S_m}\right)u_{mag}+\chi_f\right]. \tag{14}$$

Figure 8 is a plot of the magnetization, and magnetization divided by the density, of the M280 particles as a function of magnetic field strength, T. The error bars are the standard deviation of the average of the individually calculated magnetization per particle using Equation 14. Table 5 presents the data obtained in the ROI of the CTV instrument, used to make Figure 8. For field strengths greater than 0.2 T (I $\geqq$ 0.4 A), the particles were suspended in a 60% glycerin solution to reduce particle velocity to allow the magnetically induced velocity to be determined. However, this approximate 9 fold increase in viscosity resulted in a lowering of the settling velocity below the accuracy of the CTV tracking algorithm. This lack of accuracy is indicated by the large jump in CV values of the settling velocity (from ~ 0.2 to >1.0). Hence the use of Equation 14 to determine the magnetization.

The saturation behavior of the magnetization is suggestive for the use of a classic saturation model, Equation 15:

$$M\left(A-m^2/kg\right) = 7.74\left(A-m^2/kg\right)\left[\frac{B(T)}{0.0377(T)+B(T)}\right] \tag{15}$$

The solid line in Figure 8, is a non-linear fit to the data using this functional form. Inspection of Figure 8 and Equation 15, indicated that the measured, normalized magnetization of the M280 particles in this study is 7.74 A-m^2/kg, while the value reported by Fonnum et al. [15] is approximately 10.8 A-m^2/kg; a difference of approximately 28 percent. Note, we also measured an approximate 14 percent difference in densities. This relative agreement is encouraging, given that in this study, while averages are being considered when this normalized magnetization is being compared, the CTV instrument produces data on a particle by particle basis, while the vibrating magnetometer provides an average value of all of the particles on the device.

To demonstrate the potential to use the CTV instrument on particles that are significantly below typical brightfield and darkfield microscopic limits (on the order of 0.5 microns), we tested the nominally 35 nanometer, magnetic, quantum dot nanocontainers. The epifloruescent option of the microscope was used, including a mercury light source and a filter cube which was set for fluorescein isothiocynanate which is compatible with the excitation and emission of the QDOTs in the nanocontainers. The visual (microscopic) observation of the appropriate color of the QDOTs was observed and CTV code was able to track the particle movements. Figure 9 presents a histogram of the magnetically induced velocity. Since the nanocontainers are nominally 35 nanometers (too small for settling velocity measurements), the permanent magnetic assembly (S_m equal to 141×10^6 TA/m^2, $B_0 \approx 1.4$ T, dB$_0$/dx = 500 T/m) was used.

Discussion

Relationship between settling and magnetic velocities

Unlike average magnetic susceptibility data obtained from instruments, such as a SQUID or a vibrating magnetometer, single particle magnetization and size estimates were made in this study using the CTV instrument. Observations of the dot plots of settling versus magnetic velocity for the three types of magnetic particles used in this study indicates a variability in the spread of the data, depending on which particle tested, with the widest distribution observed with the EasySep particles (Figure 3A). One explanation for these results is the range of sizes; assuming that the density and magnetization of each particle is constant, Equation 4 suggests an increase of magnetic velocity with settling velocity. Consistent with this thought, the independent size measurements (using a microscope and image analysis, Figure 7) of the same particles used for CTV analysis indicates that the EasySep particles are more widely distributed with a CV of 0.488, whereas the other two types of Dynabeads have relatively uniform sizes with CVs of 0.056 and 0.024, respectively.

Effect of size distribution on magnetic and settling velocities

Given the assumption that the composition of the particles used in this study does not vary from particle to particle (i.e. the composition of specific particle types is constant), Equations 1 and 3:

$$u_{mag} = \frac{(\chi_{particle} - \chi_f) S_m}{18\eta} D_{part}^2 = \frac{\mu_0 M S_m}{B_0 18\eta} D_{part}^2 \tag{1}$$

$$u_{setl} = \frac{(\rho_{sphere} - \rho_f) g}{18\eta} D_{part}^2 \tag{3}$$

indicates that one can predict the distribution of magnetic and settling velocities given the constants, M, S_m, ρ, η and g and the relative occurrence of particle diameters using the probability distribution functions determined in Figure 7.

Figures 10A through 10C compares the model predicted distribution of settling and magnetic velocity, using probability distribution functions of the particle diameters, to the CTV measured distributions of settling and magnetic velocities, for the EasySep, M280, and M450 particles. Figures 10B and 10C present respectable fits between the model predictions (sold lines) and experimental, CTV measurements (bars). The secondary peak to the right of the main peak in magnetic velocities in Figure 10B could be due to a number of particles clumped together. Obviously, Figure 10A is a poor fit, suggesting the truncated normal distribution model is not a good model for predicting velocity distributions. Several other models were attempted without improved fit; more information is needed with respect to particle processing before further modeling approaches are attempted.

With respect to the magnetic, QDOT nanocontainers, a theoretical analysis can be made to predict the maximum, magnetically induced velocity. If one assumes that these nanocontainers are 35 nanometers in diameter, and are solid, saturated maghemite (γ-Fe_2O_3), using the previously discussed value of magnetization of 385 kA/m, the theoretical, maximum, magnetically induced velocity is given by:

$$u_{mag} = \frac{\left(\frac{\mu_0 Ms}{B_0} - \chi_f\right) D_{part}^2}{18\eta} S_m = 0.005 \ mm/s \tag{16}$$

To be tracked by the CTV code, an entity must move in a "coherent path" for at least five frames, which significantly precludes the reported velocities in Figure 9 to be the result of random motion induced by Brownian motion. Clearly, velocities significantly higher than the theoretical maximum was recorded; in addition, based on SEM photos previous reported on these types of particles, it is more likely that on the order of 10, 5 nanometers maghemite particles are contained in each nanocontainer. This corresponds to approximately 3 percent of the nanocontainer volume, or a 97% reduction in the average magnetization, which corresponds to a decrease in the magnetically induced velocity to 1.5×10^{-4} mm/s. Since a large number of entities moved faster than these theoretical calculations indicate, it is highly likely that these entities are clusters of nanocontainers. Future studies, involving other independent measurement techniques will be used to better characterize these nanocontianers in the CTV system.

Conclusions

Technologies to independently determine particle size and magnetization, in some situations, can be very valuable in the burgeoning field of nanotechnology. The majority of these particle designs are based on nano-Fe_xO_y materials, such as those used in the micron-sized particle reported here. As nanoparticle technologies approach the single particle level in sensing and manipulation applications [21–26], it will become increasingly important to characterize individual particle properties and the distribution of these properties among nanoparticles in a solution. As demonstrated in the this report, the CTV technology can not only characterize single micron sized particle, but quantify the magnetophoretic mobility of sub 500 nanometer, magnetic quantum dot nanocontainers.

Acknowledgments

Nomenclature

F	Force (N)
B	Magnetic field induction (T)
D	Diameter (m)
m	Magnetophoretic mobility (mm^3-s/kg or mm^3/T-A-s)
M_s	saturation magnetic moment of the micron particles
S_m	Magnetic energy gradient ($T \cdot A/m^2$)
V	Volume (m^3)
$1\ T$	1 N/A-m

Greek

χ	Volumetric magnetic susceptibility, SI units used (–)
η	Viscosity (kg/m-s)
μ_0	Magnetic permeability of free space (N/A^2 or T-m/A)
ρ	Density (kg/m^3)

Subscripts

|	
$\mu sphere$	Microsphere
$nano$	Nanoparticles
f	Fluid
$part$	Particle
mag	Magnetic
$setl$	Settling

References

1. Tong XD, Xiong Y, Zborowski M, Farag SS, Chalmers JJ. A novel high throughput immunomagnetic cell sorting system for potential clinical scale depletion of T cells for allogeneic stem cell transplantation. Exp Hematol. 2007; 35:1613–1622. [PubMed: 17697744]

2. Paterlini-Brechot P, Benali NL. Circulating tumor cells (CTC) detection: Clinical impact and future directions. Cancer Lett. 2007; 253:180–204. [PubMed: 17314005]

3. Yang LY, Lang JC, Balasubramanian P, Jatana KR, Schuller D, Agrawal A, Zborowski M, Chalmers JJ. Optimization of an Enrichment Process for Circulating Tumor Cells From the Blood of Head and Neck Cancer Patients Through Depletion of Normal Cells. Biotechnology and Bioengineering. 2009; 102:521–534. [PubMed: 18726961]

4. Mihajlovic G, Aledealat K, Xiong P, Von Molnar S, Field M, Sullivan GJ. Magnetic characterization of a single superparamagnetic bead by phase-sensitive micro-Hall magnetometry. Appl Phys Lett. 2007; 91

5. Bustamante C, Bryant Z, Smith SB. Ten years of tension: single-molecule DNA mechanics. Nature. 2003; 421:423–427. [PubMed: 12540915]

6. Abels JA, Moreno-Herrero F, van der Heijden T, Dekker C, Dekker NH. Single-molecule measurements of the persistence length of double-stranded RNA. Biophys J. 2005; 88:2737–2744. [PubMed: 15653727]

7. Jin XX, Yazer MH, Chalmers JJ, Zborowski M. Quantification of changes in oxygen release from red blood cells as a function of age based on magnetic susceptibility measurements. Analyst. 2011; 136:2996–3003. [PubMed: 21647486]

8. Zborowski M, Ostera GR, Moore LR, Milliron S, Chalmers JJ, Schechter AN. Red blood cell magnetophoresis. Biophysical Journal. 2003; 84:2638–2645. [PubMed: 12668472]

9. Sun J, Zborowski M, Chalmers JJ. Quantification of both the presence, and oxidation state, of Mn in Bacillus atrophaeus spores and its imparting of magnetic susceptibility to the spores. Biotechnology and Bioengineering. 2011; 108:1119–1129. [PubMed: 21449026]

10. Melnik K, Sun J, Fleischman A, Roy S, Zborowski M, Chalmers JJ. Quantification of magnetic susceptibility in several strains of Bacillus spores: Implications for separation and detection. Biotechnology and Bioengineering. 2007; 98:186–192. [PubMed: 17335063]

11. Gupta AK, Gupta M. Synthesis and surface engineering of iron oxide nanoparticles for biomedical applications. Biomaterials. 2005; 26:3995–4021. [PubMed: 15626447]

12. Jin X, Zhao Y, Richardson A, Moore L, Williams PS, Zborowski M, Chalmers JJ. Differences in magnetically induced motion of diamagnetic, paramagnetic, and superparamagnetic microparticles detected by cell tracking velocimetry. Analyst. 2008; 133:1767–1775. [PubMed: 19082082]

13. Chalmers JJ, Xiong Y, Jin X, Shao M, Tong X, Farag S, Zborowski M. Quantification of non-specific binding of magnetic micro- and nanoparticles using cell tracking velocimetry: Implication for magnetic cell separation and detection. Biotechnol Bioeng. 2010; 105:1078–1093. [PubMed: 20014141]

14. Zhang H, Moore LR, Zborowski M, Williams PS, Margel S, Chalmers JJ. Establishment and implications of a characterization method for magnetic nanoparticle using cell tracking velocimetry and magnetic susceptibility modified solutions. The Analyst. 2005; 130:514. [PubMed: 15776162]

15. Fonnum G, Johansson C, Molteberg A, Morup S, Aksnes E. Characterisation of Dynabeads by magnetization measurements and Mössbauer spectroscopy. J Magn Magn Mater. 2005; 293:41–47.

16. Chalmers JJ, Zhao Y, Nakamura M, Melnik K, Lasky L, Moore L, Zborowski M. An instrument to determine the magnetophoretic mobility of labeled, biological cells and paramagnetic particles. J Magn Magn Mater. 1999; 194:231–241.

17. Nakamura M, Zborowski M, Lasky LC, Margel S, Chalmers JJ. Theoretical and experimental analysis of the accuracy and reproducibility of cell tracking velocimetry. Exp Fluids. 2001; 30:371–380.

18. Moore LR, Zborowski M, Nakamura M, McCloskey K, Gura S, Zuberi M, Margel S, Chalmers JJ. The use of magnetite-doped polymeric microspheres in calibrating cell tracking velocimetry. J Biochem Bioph Meth. 2000; 44:115–130.

19. Ruan B, Vieira G, Henighan T, Chen A, Thakur D, Sooryakumar R, Winter JO. Simultaneous Magnetic Manipulation and Flourescent Tracking of Multiple Individual Hybrid Nanostructures. Nano Lett. 2010; 10:2220–2224. [PubMed: 20450169]

20. Woo K, Hong J, Choi S, Lee HW, Ahn JP, Kim CS, Lee SW. Easy synthesis and magnetic properties of iron oxide nanoparticles. Chem Mater. 2004; 16:2814–2818.

21. Park JH, von Maltzahn G, Ruoslahti E, Bhatia SN, Sailor MJ. Micellar hybrid nanoparticles for simultaneous magnetofluorescent imaging and drug delivery. Angew Chem Int Ed Engl. 2008; 47:7284–7288. [PubMed: 18696519]

22. Selvan ST, Patra PK, Ang CY, Ying JY. Synthesis of Silica-Coated Semiconductor and Magnetic Quantum Dots and Their Use in the Imaging of Live Cells. Angewandte Chemie International Edition. 2007; 46:2448–2452.

23. Insin N, Tracy JB, Lee H, Zimmer JP, Westervelt RM, Bawendi MG. Incorporation of Iron Oxide Nanoparticles and Quantum Dots into Silica Microspheres. ACS Nano. 2008; 2:197–202. [PubMed: 19206619]

24. Deng S, Ruan G, Han N, Winter JO. Interactions in fluorescent-magnetic heterodimer nanocomposites. Nanotechnology. 2010; 21:145605. [PubMed: 20215661]

26. Gu H, Zheng R, Zhang X, Xu B. Facile One-Pot Synthesis of Bifunctional Heterodimers of Nanoparticles: A Conjugate of Quantum Dot and Magnetic Nanoparticles. J Am Chem Soc. 2004; 126:5664–5665. [PubMed: 15125648]
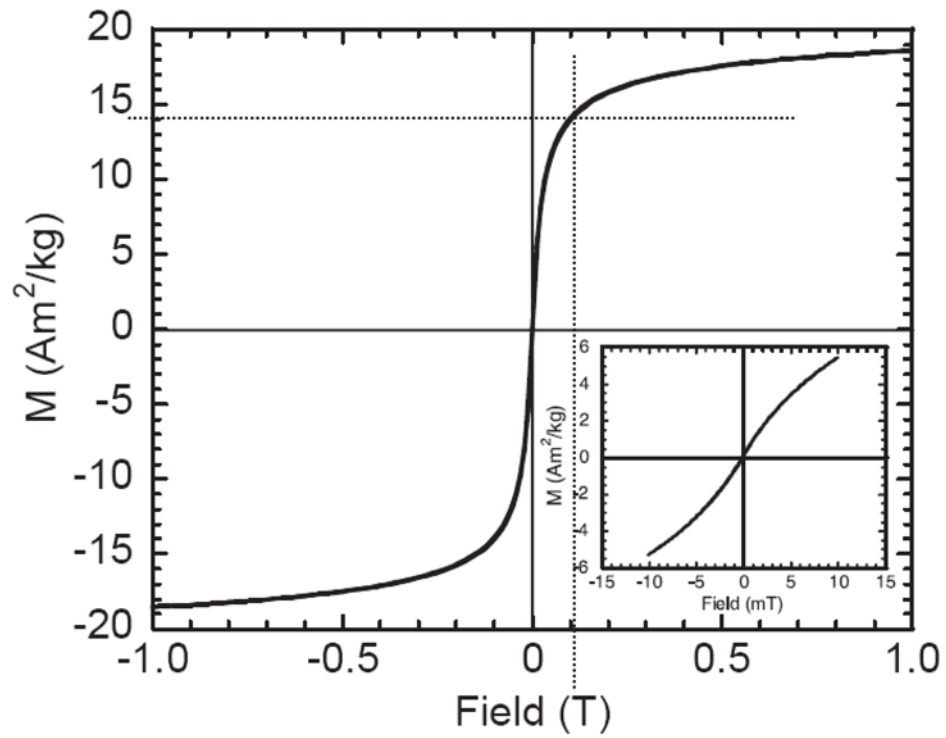
1A
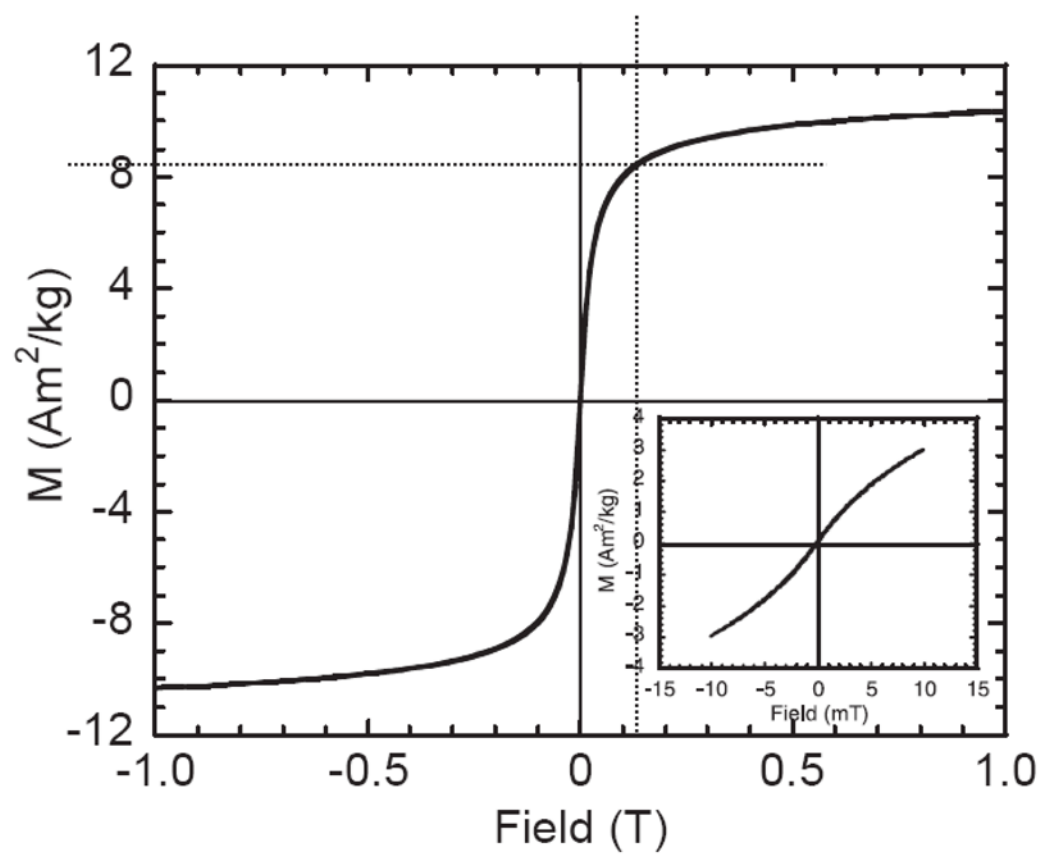
1B

Figure 1.
Magnetization versus magnetic field at room temperature for Dynal M-280, 1A and M-450, 1B in the magnetic field range of 0 to ± 1.0 T. Inserted figures show the hysteresis loops in the field range 0 ± 710 mT. The vertical dotted lines correspond to the magnetic field strength in the low power CTV system. (Adapted from Fonnum *et al.* 2005).
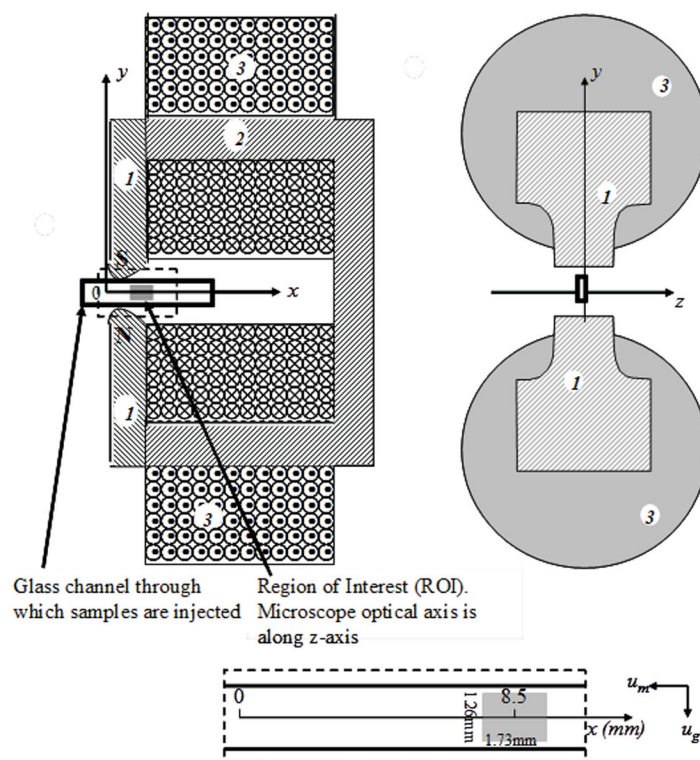
Figure 2.
Schematic diagram of the relative position of the electric coils and analysis channel for the electromagnetic CTV system. 1, 2 — pole pieces and flux return yolk made of 1018 low-carbon steel; 3 — copper wire coil.
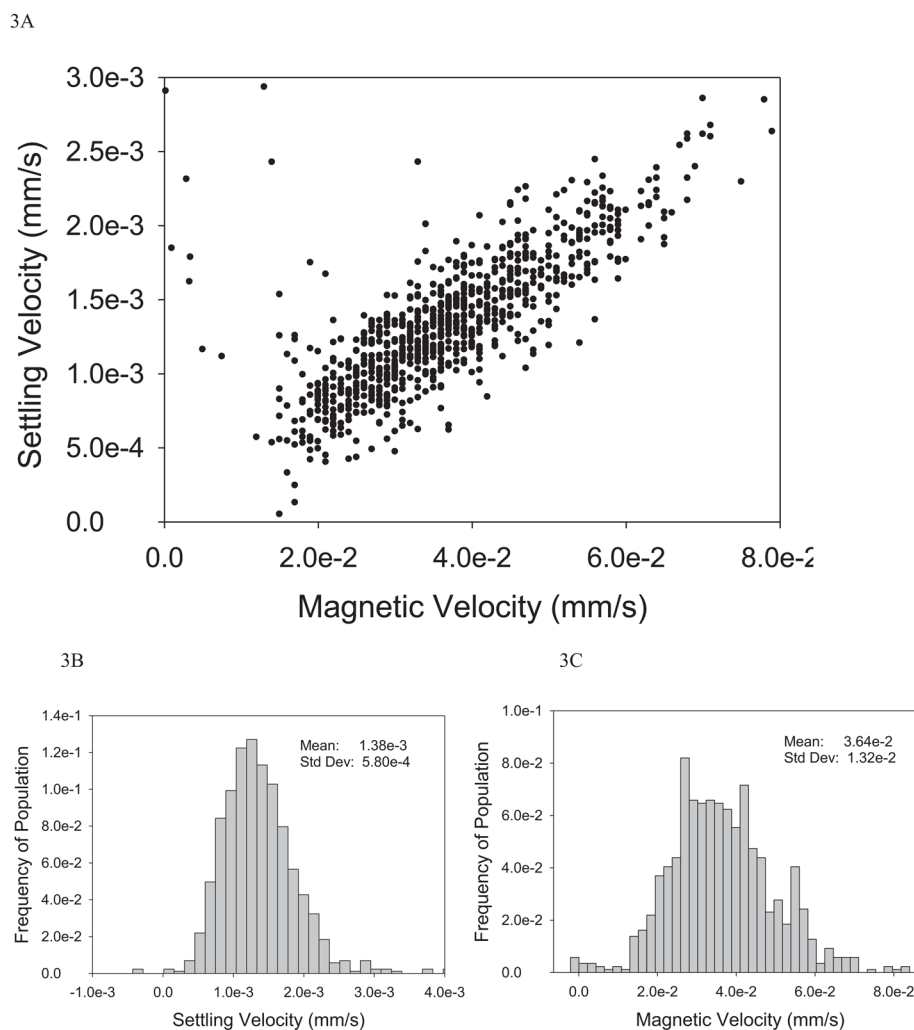
3A

3B

3C

Figure 3.
Dot plot, 3A, and histograms of the settling velocity and magnetic velocity, 3B and 3C, respectively, of EasySep D magnetic particles (Stem Cell Technologies Inc. 19250) using the electromagnet CTV (0.2A; $S_m = 0.84$ TA/mm^3).
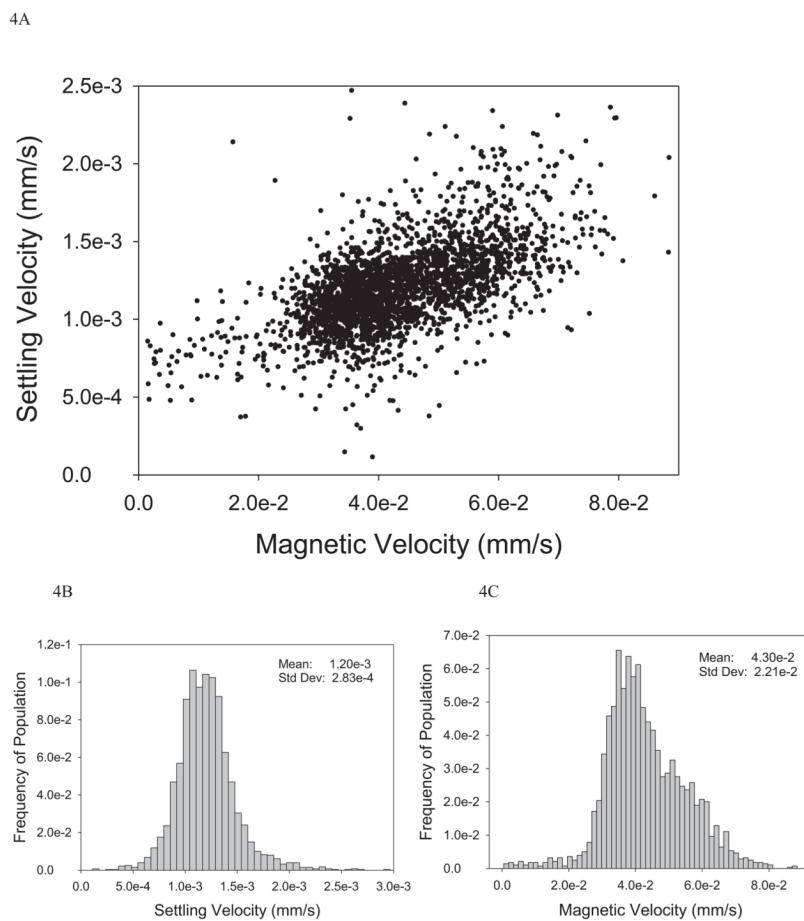
4A

4B 4C

Figure 4.
Dot plot,4A, and histograms of the settling velocity and magnetic velocity, 4B and 4C, respectively, of Dynal M280 magnetic particles using the electromagnet CTV (0.2A; S_m = 0.84 TA/mm^3).
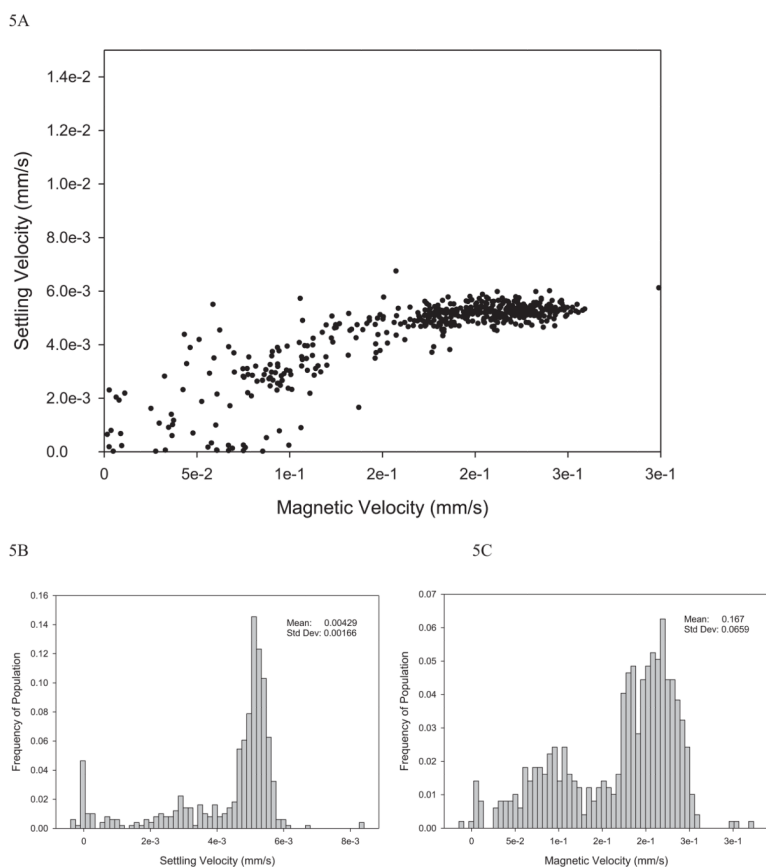
5A

5B

5C

Figure 5.
Dot plot, 5A, and histograms of the settling velocity and magnetic velocity, 5B and 5C, respectively, of the Dynal M450 particles in PBS solution using the electromagnet CTV (0.2A; S_m = 0.84 TA/mm^3).
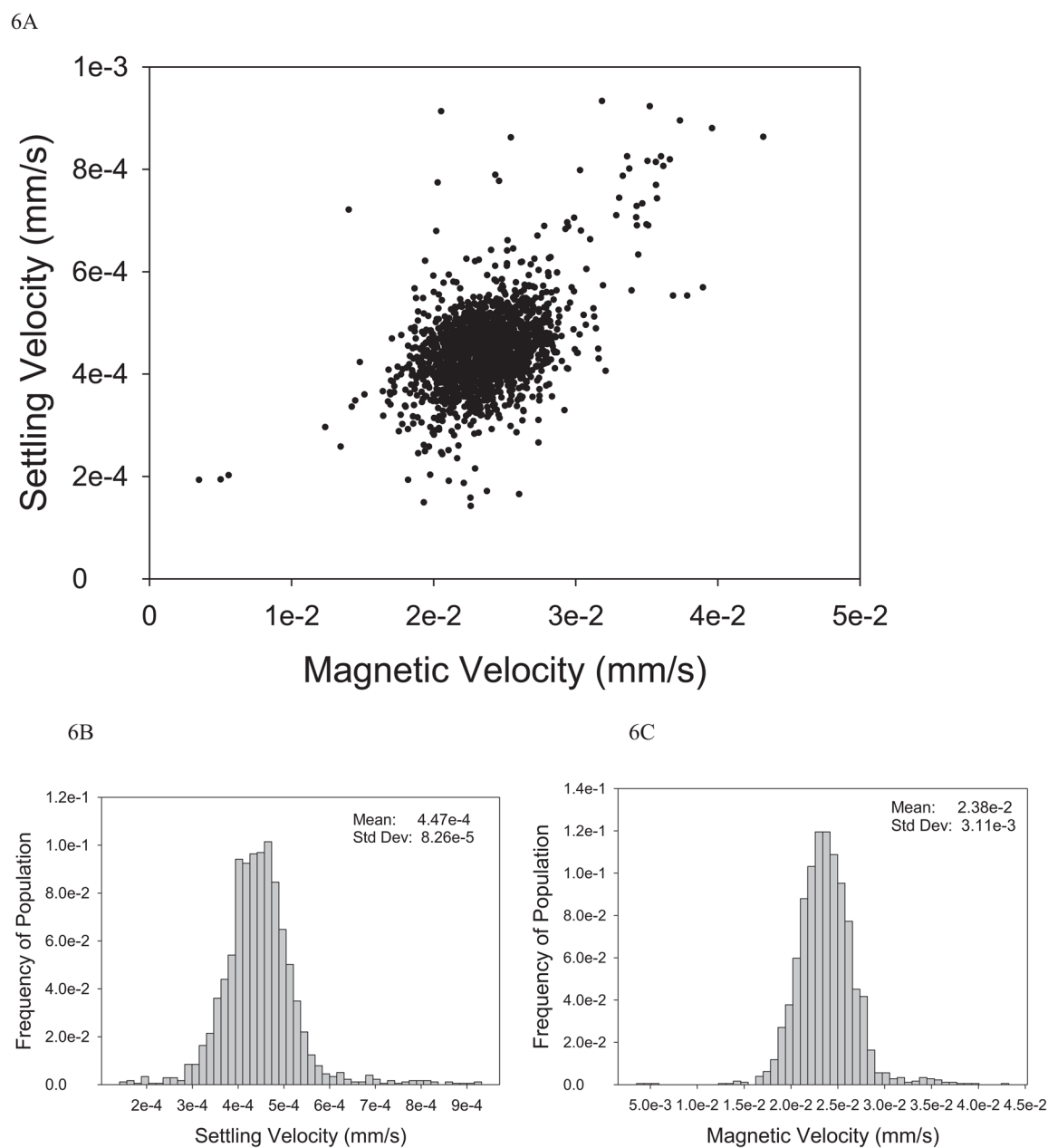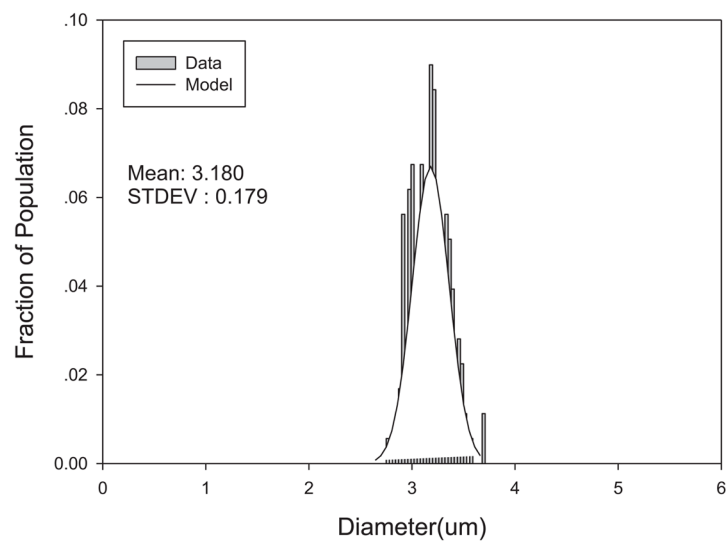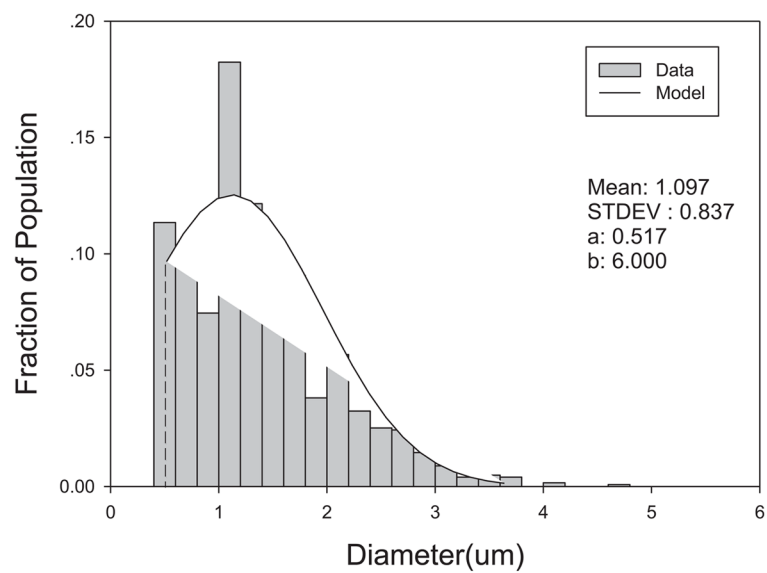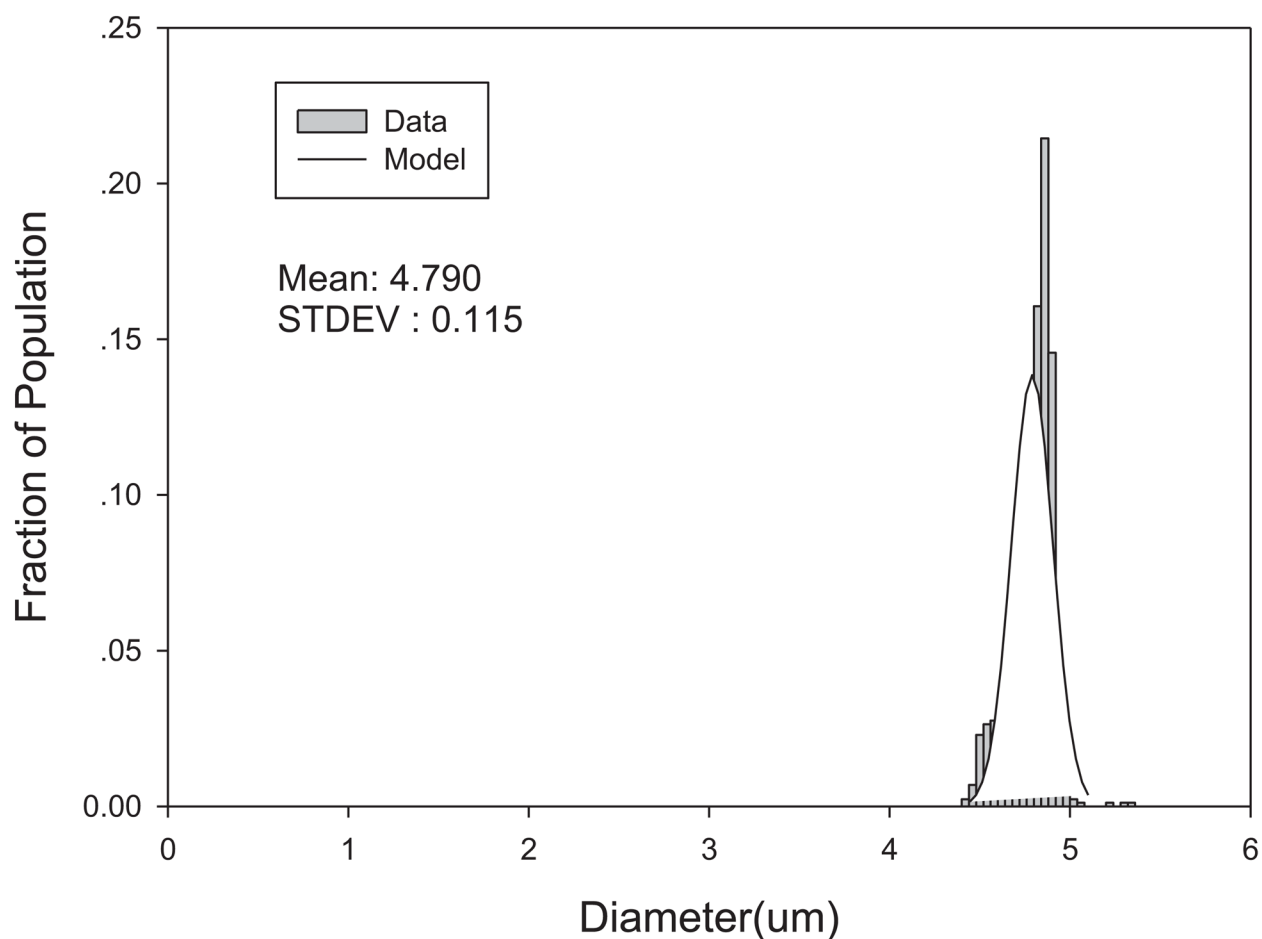
6A

6B

6C

Figure 6.
Dot plot, 6A, and histograms of the settling velocity and magnetic velocity, 6B and 6C, respectively, of the Dynal M450 particles in 60 wt % glycerol solution using the electromagnet CTV (0.2A; S_m= 0.84 TA/mm ^{3}).

7A

7C

Figure 7.
Histograms of the diameter of the Stem Cell Technologies particles, Figure 7A, the M280 Dynal particles, 7B, and M450 Dynal particles, Figure 7C. Data obtained using a Nikon 80i microscope and the NIS Elements BR research software. The truncated normal distribution and normal distribution are used to fit the data, the numerical parameters presented in the figure represents the constant used in the model.
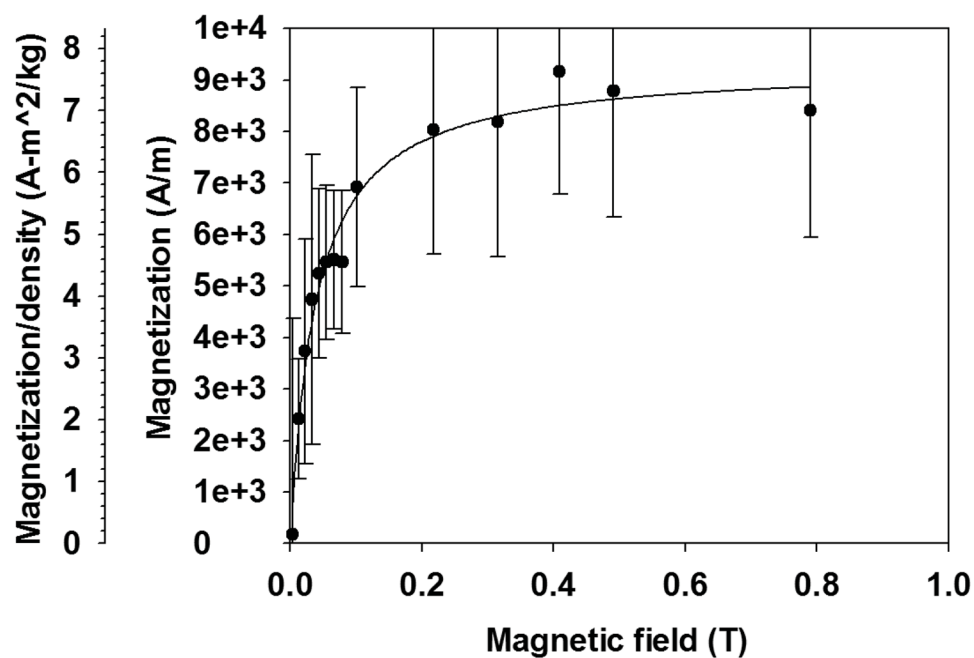
Figure 8.
Magnetization, and magnetization divided by density, as a function of magnetic field in the ROI of the CTV system for the M280 particles.
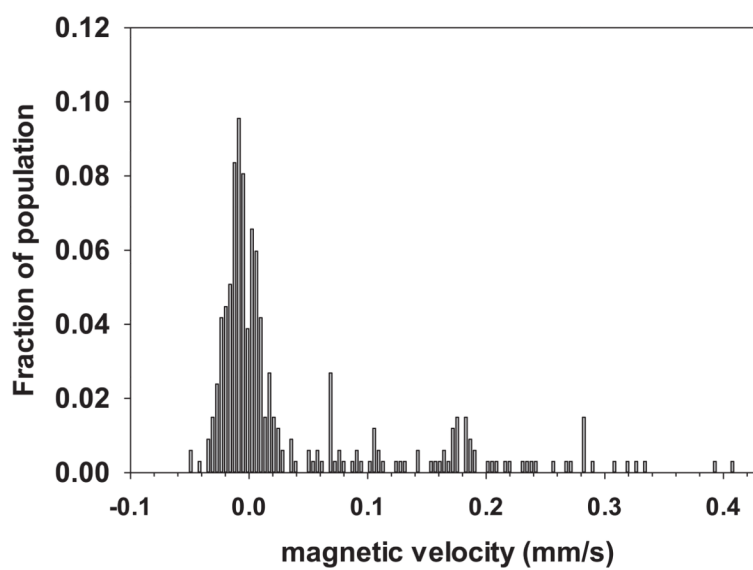
Figure 9.
Histogram of magnetically induced velocity of magnet quantum dots.
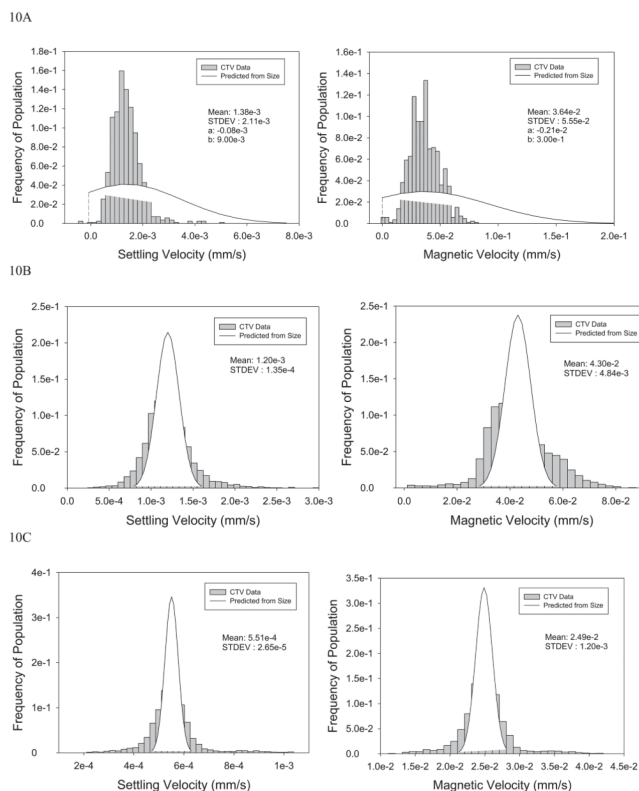
Figure 10.
Comparison of magnetic velocities and settling velocities of the Stem Cell Technologies particles, Figure 10A, the M280 Dynal particles, 10B, and M450 Dynal particles, Figure 10C, between experimental data from CTV measurements (vertical bars) and predicted velocity distribution using the distribution models obtained from particle size measurements.

Table 1

Volumetric magnetic susceptibilities of relevant compounds (Adapted from [14])

Compound	Formula	Magnetic susceptibility $\chi (\times 10^{-6})$
Water	H_2O	−9.05
D-Glucose	$C_6H_{12}O_6$	−10.92
Maghemite,	γ-Fe_2O_3	$2 \sim 2.5 \times 10^6$
Hematite	α-Fe_2O_3	$500 \sim 40,000$
Magnetite	$2Fe_2O_3 \cdot FeO$	$1 \sim 5.7 \times 10^6$

Table 2

Three types of commercially available micron sized magnetic particles studied in this paper

Particle	Manufacturer Cat #	Reported Diameter (microns)	Reported density (kg/m³)
Dynabeads M-280	Invitrogen 658.01D	2.83	1,400
Dynabeads M-450	Invitrogen 111.51D	4.4	1,600
EasySep D	Stem Cell Technologies Inc. 19250	Not reported	Not reported

Table 3

The mean and coefficient of variation of settling and magnetic velocity, and the quotient of magnetic and settling velocity of the magnetic particles analyzed.

Particle	Mean settling velocity (mm/s)	CV	Mean magnetic velocity (mm/s)	CV	u_{mag}/u_{settle}	CV
EasySep D	1.38×10^{-3}	0.42	3.64×10^{-2}	0.36	28.3	0.44
Dynabeads M-280	1.20×10^{-3}	0.23	4.30×10^{-2}	0.51	36.5	0.33
Dynabeads M-450 (buffer)	4.29×10^{-3}	0.39	1.67×10^{-1}	0.40	122	35
Dynabeads M-450 (glycerol)	4.47×10^{-4}	0.19	2.38×10^{-2}	0.13	36.5	0.33

Table 4

The visually measured diameter, calculated density, magnetization, and average magnetic content in the particles

	Mean diameter microscopically measured in this study (microns)	CV of measured diameter	Mean density (kg/m³)	Magnetization (A/m)	Average volume fraction maghemite (%)	Average number of grams per particle
EasySep D	1.38	0.488	2.2×10^3	3.24×10^4	10	6.3×10^{-13}
Dynabeads M-280	3.18	0.056	1.20×10^3	6.85×10^3	2.1	1.6×10^{-12}
Dynabeads M-450 (glycerol)	4.79	0.024	1.39×10^3	1.69×10^4	5.3	1.4×10^{-11}

Table 5

The data obtained in the ROI of the CTV instrument

Current (A)	B(T)	S_m (TA/mm²)	Number of particles tracked	Mean settling velocity (mm/s)	CV	Mean magnetic velocity (mm/s)	CV	Magnetization (A/m)	Magnetization/density (Am²/kg)
0.02	3.53E-03	1.03E-03	889	1.33E-03	0.214	3.84E-05	24.1	174	0.145
0.04	1.23E-02	1.23E-02	1220	1.26E-03	0.208	1.83E-03	0.483	2420	2.01
0.06	2.22E-02	3.98E-02	1019	1.17E-03	0.210	5.05E-03	0.345	3730	3.10
0.08	3.31E-02	8.75E-02	1165	1.13E-03	0.224	9.46E-03	0.297	4740	3.95
0.1	4.34E-02	1.51E-01	977	1.09E-03	0.241	1.38E-02	0.314	5240	4.36
0.12	5.48E-02	2.40E-01	1090	1.21E-03	0.218	1.80E-02	0.275	5460	4.54
0.14	6.57E-02	3.50E-01	561	1.25E-03	0.187	2.54E-02	0.245	5510	4.59
0.16	7.86E-02	4.93E-01	679	1.36E-03	0.203	3.12E-02	0.254	5460	4.54
0.2	1.01E-01	8.36E-01	2793	1.20E-03	0.229	4.30E-02	0.280	6920	5.76
0.4	2.17E-01	3.78E+00	1757	4.16E-05	2.03	1.11E-02	0.289	8040	6.69
0.6	3.15E-01	8.04E+00	1355	4.69E-05	1.90	1.66E-02	0.309	8190	6.81
0.8	4.09E-01	1.33E+01	3517	2.62E-05	2.83	2.32E-02	0.269	9160	7.63
1	4.91E-01	1.91E+01	1720	3.96E-05	2.18	2.68E-02	0.289	8780	7.31
2	7.90E-01	5.09E+01	1212	3.03E-05	3.36	4.25E-02	0.289	8410	7.00

1) Equations for single particle magnetization and size based presented

2) Magnetization and size a commercial magnetic particles experimentally measured

3) Magnetization vs field determined